ACADEMIC PRESS

Available online at www.sciencedirect.com

SCIENCE DIRECT®

Journal of Sound and Vibration 269 (2004) 19–31

JOURNAL OF SOUND AND VIBRATION

www.elsevier.com/locate/jsvi

Modal characteristics of a flexible beam with multiple distributed actuators

N.D. Maxwell[a,*], S.F. Asokanthan[b]

[a] *Department of Mechanical Engineering, The University of Queensland, Queensland 4072, Australia*
[b] *Department of Mechanical and Materials Engineering, The University of Western Ontario, Ont., Canada N6A 5B9*

Received 25 February 2002; accepted 10 December 2002

Abstract

A flexible structure with surface-bonded piezoceramic patches is modelled using Timoshenko beam theory. Exact mode shapes and natural frequencies associated with the flexural motion are computed for various piezoceramic distributed actuator arrangements. The effects of patch placement and of shear on the modal characteristics are demonstrated using a cantilevered beam as an example. Perfect bonding of the piezoceramic to the beam substructure is assumed, and for the purposes of this paper only passive piezoceramic properties are considered. The modelling technique and results obtained in a closed form are intended to assist investigations into the modelling and control of active structures with surface-bonded piezoceramic actuators.

1. Introduction

The use of distributed actuators for active vibration damping has been a topic of considerable recent interest in the field of structural vibration control. Often structures must sacrifice stiffness in order to achieve reduced weight requirements, for example in aerospace applications. However, low stiffnesses can result in structures vulnerable to vibrations and hence in reduced performance levels. In order to suppress vibration while retaining the desired low structural masses, smart structures using distributed actuation are currently being researched. One method of achieving distributed actuation for vibration damping is through the use of bonded piezoceramic actuators. However, piezoceramic actuators possess significant mass and flexural rigidity, and can significantly alter the dynamic behaviour of the structures they are bonded to. Therefore, it is

*Corresponding author.
E-mail addresses: maxwell@mech.uq.edu.au (N.D. Maxwell), sasokanthan@eng.uwo.ca (S.F. Asokanthan).

0022-460X/03/$ - see front matter
doi:10.1016/S0022-460X(02)01604-8

important to include changes in beam characteristics due to piezoceramic patch placement into dynamic models of vibrating structures.

Crawley and deLuis [1] and Garcia et al. [2], amongst others, investigated the active sensing and actuation of vibrating structures using piezoelectric materials. However, early investigations typically neglected the effects of the piezoelectric materials themselves on the modal characteristics of structures. The assumption of negligible behavioural effects is acceptable for low ratios of piezoelectric to substructure thickness, as in the case of structures bonded with PVDF actuators (see, e.g., Ref. [3]). However, thick piezoelectrics such as PZTs (lead zirconate titanates) tend to stiffen structures and can significantly affect the dynamic behaviour. Due to their large masses and costs, it is also desirable to limit the sizes of piezoceramic actuators. However, this results in non-uniform structural properties, which further complicate the vibration behaviour.

Some recent studies have included the dynamic effects of localized piezoceramics into their vibration models. Yang and Lee [4] determined the mode shapes of a stepped cantilever beam with a single PZT actuator at the fixed end of the beam. Chan and Wang [5] modelled the more general case of a cantilever beam with arbitrary placement of a single distributed mass, but did not include the effects of distributed flexural rigidity. Chan et al. [6] extended this work to include the effects of multiple distributed masses. Joshi [7] considered vibration characteristics of rockets including the effects of mass depletion and of axial compression. Recently, Aldraheim et al. [8] investigated practical considerations for optimal piezoceramic placement and sizing for various boundary conditions, including the effects of both distributed mass and distributed flexural rigidity, but focused on optimization rather than modelling. The present investigation extends the work of Chan et al. [6] to include the effects of distributed flexural rigidity on the modes of vibration and to provide accurate closed-form dynamic models of beam with multiple patches for the purposes of controller design.

In this paper, a generic model for a vibrating cantilever beam with surface-bonded piezoceramic patches is derived from Timoshenko beam theory and Hamilton's Principle. Assuming separability of time and space variables facilitates prediction of exact frequencies and modes shapes. A tip mass term is included in the model to represent the possible presence of a payload or tip sensor in typical applications. Non-uniform beam properties are included by modelling beams using equivalent sets of connected beam segments. These beam segments are of equal length and each possess uniform material properties. This method generates separate mode shapes for each segment that when placed end-to-end yield overall system mode shapes. It also means any arrangement of PZTs may be modelled and allows PZT sizes to be unconstrained. Finally in this paper, numerical examples are presented and the effects of patch placement on the modal characteristics are discussed. The method and analysis presented in this paper can also be applied to beams subject to other boundary conditions without much difficulty.

2. Modelling

The classical one-dimensional Euler–Bernoulli equation for the flexural vibration of beams is the simplest model available for representing the flexural motion of elastic beams. However, this model is known to be inaccurate, especially for higher modes of vibration. It neglects factors that

can influence the modal characteristics such as the effects of the cross-sectional dimensions. The Timoshenko model refines the Euler–Bernoulli model by including shear deformation and rotatory inertia effects. In the present study, Timoshenko beam theory is used to model a cantilever beam with tip mass configuration.

For the beam differential element shown in Fig. 1, the angle of rotation due to bending is represented by space and time-dependent angle $\psi(x,t)$, the shear force by Q and the bending moment by M. Shear distortion is caused by the deformation of the beam due to the shear stress, and is represented by space and time-dependent angle $\beta(x,t)$ that influences the slope of the elastic axis. The angles $\psi(x,t)$ and $\beta(x,t)$ make up the total angular distortion, which can be described by

$$\frac{\partial w(x,t)}{\partial x} = \psi(x,t) + \beta(x,t), \tag{1}$$

where $w(x,t)$ represents the deflection of the beam.

2.1. Equations of motion

The equations of motion of the flexible beam can be derived using the extended Hamilton's Principle (see, e.g., Ref. [9]). Partial differential equations that govern the motion of a flexible beam as given by Timoshenko beam theory are:

$$\frac{\partial}{\partial x}\left[(EI)_s\frac{\partial \psi_s}{\partial x}\right] + k'G_sA_s\left(\frac{\partial w_s}{\partial x} - \psi_s\right) - (\rho I)_s\frac{\partial^2 \psi_s}{\partial t^2} = 0, \tag{2}$$

$$\frac{\partial}{\partial x}\left[k'G_sA_s\left(\frac{\partial w_s}{\partial x} - \psi_s\right)\right] - (\rho A)_s\frac{\partial^2 w_s}{\partial t^2} = 0, \tag{3}$$

where subscripted s is used to distinguish between different beam segments, k' is the shear coefficient dependent on the cross-sectional area, EI is the flexural stiffness, A is the area, ρ is the mass per unit length, and G is the shear modulus. Eliminating ψ_s and w_s, respectively, from Eqs. (3) and (4), the following differential equations in w_s and ψ_s may be derived (see, e.g., Ref. [10]):

$$(EI)_s\frac{\partial^4 w_s}{\partial x^4} + (\rho A)_s\frac{\partial^2 w_s}{\partial t^2} - \left((\rho I)_s + \frac{(\rho A)_s(EI)_s}{k'G_sA_s}\right)\frac{\partial^4 w_s}{\partial x^2\,\partial t^2} + (\rho I)_s\frac{(\rho A)_s}{k'G_sA_s}\frac{\partial^4 w_s}{\partial t^4} = 0, \tag{4}$$

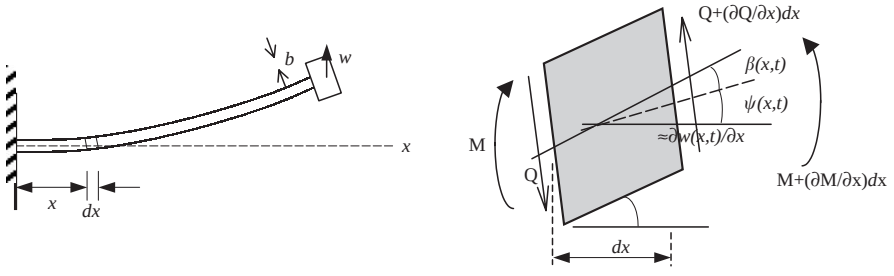

Fig. 1. Timoshenko beam element.

$$(EI)_s\frac{\partial^4\psi_s}{\partial x^4}+(\rho A)_s\frac{\partial^2\psi_s}{\partial t^2}-\left((\rho I)_s+\frac{(\rho A)_s(EI)_s}{k'G_sA_s}\right)\frac{\partial^4\psi_s}{\partial x^2\,\partial t^2}+(\rho I)_s\frac{(\rho A)_s}{k'G_sA_s}\frac{\partial^4\psi_s}{\partial t^4}=0. \tag{5}$$

Assuming separability of time and space variables and setting $w_s(x,t)=\Phi_s(x)e^{j\omega t}$ in Eq. (5), the characteristic equation in the spatial co-ordinate Φ that describes the deflection is obtained as

$$\Phi_s^{iv}-\lambda_s^4\Phi_s+2(p_s+q_s)\Phi_2''+4p_sq_s\Phi_s=0, \tag{6}$$

where

$$\lambda_s^4=\frac{(\rho A)_s\omega^2}{(EI)_s},\quad p_s=\frac{(\rho I)_s\omega^2}{2(EI)_s},\quad q_s=\frac{(\rho A)_s\omega^2}{2k'G_sA_s}.$$

Setting $\psi_s(x,t)=\Psi_s(x)e^{j\omega t}$ in Eq. (6) yields an identical characteristic equation for ψ, the spatial co-ordinate that describes the angular rotation. From the characteristic equations, solutions may be obtained of the form

$$\Phi_s(x)=A_s\sin\alpha_sx+B_s\cos\alpha_sx+C_s\sinh\beta_sx+D_s\cosh\beta_sx, \tag{7}$$

$$\Psi_s(x)=-f_{\alpha s}B_s\sin\alpha_sx+f_{\alpha s}A_s\cos\alpha_sx+f_{\beta s}D_s\sinh\beta_sx+f_{\beta s}C_s\cosh\beta_sx, \tag{8}$$

$$f_{\alpha s}=\frac{1}{\alpha_s}\left(\alpha_s^2-\frac{\rho_sA_s}{k'A_sG_s}\omega^2\right),\quad f_{\beta s}=\frac{1}{\beta_s}\left(\beta_s^2+\frac{\rho_sA_s}{k'A_sG_s}\omega^2\right) \tag{9}$$

and the parameters α_s and β_s are defined by $\alpha_s^2=(p_s+q_s)+\sqrt{(p_s-q_s)^2+\lambda_s^4}$ and $\beta_s^2=-(p_s+q_s)+\sqrt{(p_s-q_s)^2+\lambda_s^4}$.

2.2. Boundary conditions

Modelling of the non-uniform composite beam is performed using segmentation to produce component mode shapes for each beam section. The resulting mode shapes are assembled to obtain the system mode shapes of the beam. In this research, segments of equal length are used, however the principle applies equally well to variable segment sizes. Also, since consecutive patches next to each other are modelled as equivalent to single large patches, small segment sizes can therefore be used to get single PZTs of any length. This discretized approach has been found to be useful for iterative problems such as optimal patch placement, where patch length may be unknown. In the generic model presented in this document, patches are constrained to match the segment lengths and are then specified as either present or absent for each segment. This means that regardless of whether piezoceramics are present or absent, each beam segment always possesses uniform internal beam properties.

The fixed-end boundary conditions of a cantilever beam are

$$w_1(0,t)=0\quad\text{and}\quad\psi_1(0,t)=0.$$

Between beam segments, the compatibility conditions are:

$$w_s(\mu_s^-,t)=w_{(s+1)}(\mu_s^+,t),$$

$$\psi_s(\mu_s^-,t)=\psi_{(s+1)}(\mu_s^+,t),$$

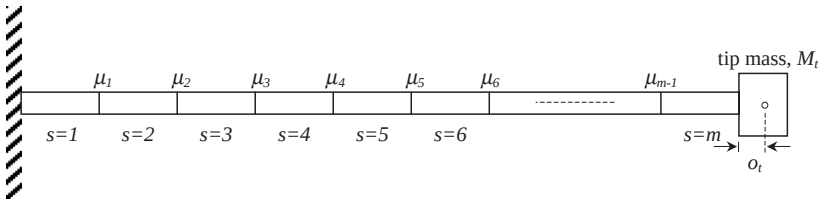

Fig. 2. Beam segmentation.

$$(EI)_s(\partial\psi_s(x,t)/\partial x)_{x=\mu_s^-} = (EI)_{(s+1)}(\partial\psi_{(s+1)}(x,t)/\partial x)_{x=\mu_s^+},$$

$$k'G_sA_s(\partial w_s(x,t)/\partial x - \psi_s(x,t))_{x=\mu_s^-} = k'G_{(s+1)}A_{(s+1)}(\partial w_{(s+1)}(x,t)/\partial x - \psi_{(s+1)}(x,t))_{x=\mu_s^+}.$$

In these compatibility equations, the boundaries considered occur between segments s and $(s+1)$, counting from $s=1$ for the segment at the fixed end to $s=m$ at the tip as shown in Fig. 2. The symbol μ_s is used to indicate the positions along x at which the division boundaries are located. If m segments of equal length are considered we can therefore define $\mu_s = sL/m$.

With the inclusion of a tip mass offset o_t, the tip boundary conditions can be shown to be (see, e.g., Refs. [11,12])

$$(EI)_m(\partial\psi_m(x,t)/\partial x)_{x=L} = -(I_t + M_to_t^2)(\partial^2\psi_m(L,t)/\partial t^2) - M_to_t(\partial^2 w_m(L,t)/\partial t^2),$$

$$k'G_mA_m(\partial w_m(x,t)/\partial x - \psi_m(x,t))_{x=L} = -M_t(\partial^2 w_m(L,t)/\partial t^2) - M_to_t(\partial^2\psi_m(L,t)/\partial t^2).$$

Substituting the general expressions (7) and (8) for the mode shapes into these boundary conditions yields

$$[F(\omega)]V = 0, \tag{10}$$

where $[F(\omega)]$ is the characteristic matrix of size $(4\,\mathrm{m}\times 4\,\mathrm{m})$, m being defined as the number of segments (of equal or unequal length) the beam is divided into, and

$$V = [A_1\ B_1\ C_1\ D_1\ A_2\ B_2\ C_2\ D_2 \cdots A_m\ B_m\ C_m\ D_m]^{\mathrm{T}}$$

is the coefficient vector to be determined. The natural frequencies then correspond to the eigenvalues of the characteristic matrix and hence can be found from

$$Q(\omega) = \det|F(\omega)| = 0. \tag{11}$$

The corresponding eigenvectors can then be obtained by substituting ω_i into $[F(\omega)]$ and solving the eigenvalue problem:

$$[F(\omega_i)]V_i = \Lambda_i V_i, \tag{12}$$

where Λ_i are the eigenvalues of $[F(\omega_i)]$. The resultant eigenvectors V_i then represent the vector of mode shape constants for mode i.

3. Results and analysis

Mode shapes and natural frequencies will be computed for various arrangements of single- and multiple-patch piezoceramic configurations. These natural frequencies will be compared against those of the beam alone. Consideration of the effects of shear will be performed using comparisons between results obtained using the Timoshenko beam model and the Euler–Bernoulli beam model. The effects of varying the shear parameter value will also be considered.

3.1. Modal analysis

For the purposes of this analysis configurations using multiple segments of equal length are used. All configurations are represented using binary notation, where the number of digits is the same as the number of segments of equal length that the beams are divided into. The first digit in the binary number describes the segment closest to the fixed end and the final digit describes the segment closest to the tip, and a '1' indicates a PZT present on the segment described while a '0' indicates no PZT present. The patch placement shown in Fig. 3 can therefore be described as '0110111000' and can describe two patches present, one from $0.1L$ to $0.3L$ and the other from $0.4L$ to $0.7L$.

The first two system mode shapes for a cantilevered beam divided into two segments are included in Fig. 4 for each of the following configurations: no piezoceramics present ('00'), a single piezoceramic present at the hub end of the beam only ('10'), and a single piezoceramic present at the tip end of the beam only ('01'). The beam and PZT properties used in this study are listed in Table 1. From these simple configurations qualitative understanding of the effects of distributed masses and stiffnesses on beam vibration may be attained. For example, Fig. 4(b) demonstrates that when piezoceramic patches are placed over the region from $x/L = 0$ (the hub) to $x/L = 0.5$ as for the '10' case, the resultant additional stiffening reduces the second mode deflection in this region and increases it elsewhere. The peak of bending also relocates to $x/L \approx 0.55$, outside the piezoceramic region. When a patch is placed over the region from $x/L = 0.5$ to $x/L = 1$ (the tip) as for the '01' case, the peak shifts to $x/L \approx 0.45$, again outside the piezoceramic region.

The effects of patch placement on the natural frequencies of vibration are also noted in the legend in Fig. 4 using non-dimensional frequency ratios. The frequencies for each configuration

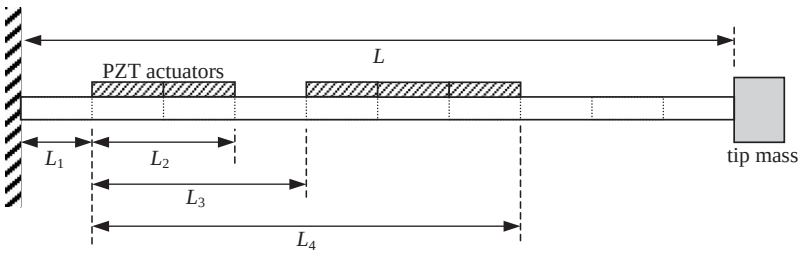

Fig. 3. Segmented cantilever beam with tip mass and distributed actuators.

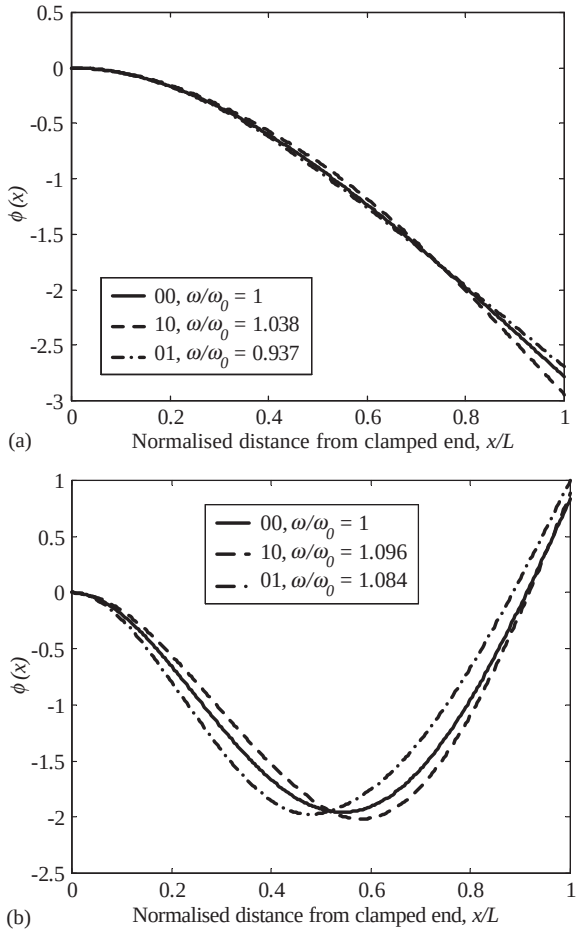

Fig. 4. Comparisons of mode shapes of deflection using various two segment piezoceramic configurations for (a) mode 1 vibration and (b) mode 2 vibration. Deflection plots are scaled for unity integrals.

Table 1
Beam and piezoceramic properties

Property	Beam	Piezoceramics
Height, h	0.05 m	0.05 m
Breadth, b	0.004 m	0.002 m
Density, ρ	7800 kg/m^3	7700 kg/m^3
Length, L	0.30	—
Young's modulus, E	193 GPa	62 GPa
Shear modulus, G	74 GPa	23.8 GPa
Tip mass, M_t	0.036 kg	—
Tip offset, o_t	0.008 m	—

are compared to the natural frequency ω_0 associated with the case for no PZT actuators. For mode 1, the majority of bending occurs close to the hub, so a patch placed in this region tends to stiffen the beam against vibration and hence raises the natural frequency, as in the '10' case. Since little bending for this mode occurs towards the tip, a patch in this region as in the '01' case does little to stiffen the beam but instead acts as an additional tip mass, reducing the natural frequency. For mode 2 vibration, larger curvature change occurs approximately in the regions of x/L from 0 to 0.2 and 0.4 to 0.6 than elsewhere. Therefore both the '10' and '01' PZT configurations contribute to beam stiffening and hence raise the natural frequency.

However, while some intuitive understanding of the effects of patch placement on vibration can be achieved from inspection in this way, PZTs at all times contribute to both stiffness and mass. The above observations demonstrate that the presence of PZT patches significantly alters the modal characteristics of the composite structure. Hence, it is important when performing quantitative vibration analyses and dynamic modelling of multiple patch configurations to perform exact numerical computations using methods such as the one presented in this document.

A typical arrangement used for investigating more than two segments is illustrated in Fig. 3. This particular arrangement can represent either five small patches each of length $0.1L$ or two larger patches of length $0.2L$ and $0.3L$ respectively. Any desired patch arrangement may also be represented in this form. In Fig. 3, L_1 is the distance from the fixed end to the first PZT, L_2 is the length of the first PZT, L_3 is the distance between the start of the first PZT and the start of the second PZT, and L_4 is the distance between the start of the first PZT and the end of the second PZT. These variables are useful in analysing the beam vibration behaviour for two bonded PZTs of variable lengths.

The dynamic behaviour of the first four modes of vibration for various patch configurations is characterized using the frequency ratios provided as Fig. 5, with the associated mode shapes shown in Fig. 6. Here ω_0 represents the fundamental natural frequency of the beam substructure (i.e., for a configuration represented by '0000000000'), while ω represents the frequency of the composite structure. Plots of the first few mode shapes for a few different configurations normalized such that the integrals of the shapes with respect to the spatial co-ordinate are unity.

Two cases are presented here. Fig. 5(a) details the frequency ratios for the case of a single patch of varying length. Fig. 5(b) details the case of two patches present, where one patch has a fixed length of $0.2L$ and the length of the other patch varies. These results may be compared to those presented by Chan et al. [6], who investigated the effects of distributed mass on the modal characteristics but did not include flexibility effects. They observed that the frequency ratios for similar configurations decreased for increasing distributed mass sizes, which may be attributed to inertial effects. However, in the present study, attempts have been made to include the effects of patch flexibility on the modal characteristics in order to investigate their significance.

In the study by Chan et al. [6], plateaus were observed in the frequency ratios for variable normalized length $(L_4 - L_3)/L$. It was theorized that the number of these plateaus corresponded to the number of nodes covered by the distributed mass. In Figs. 5(a) and (b), and from the corresponding mode shapes in Fig. 6, it may be seen by close inspection that the natural frequencies increase when PZTs are located in regions of high modal flexure and decrease when PZTs are located in regions of low flexure. For example, the mode 1 frequency ratio in Fig. 5(a) peaks at $(L_4 - L_3)/L = 0.5$. The gradient of this frequency ratio plot is steepest for normalized lengths of approximately 0 and 0.9. At the peak, a single patch may be considered to extend over

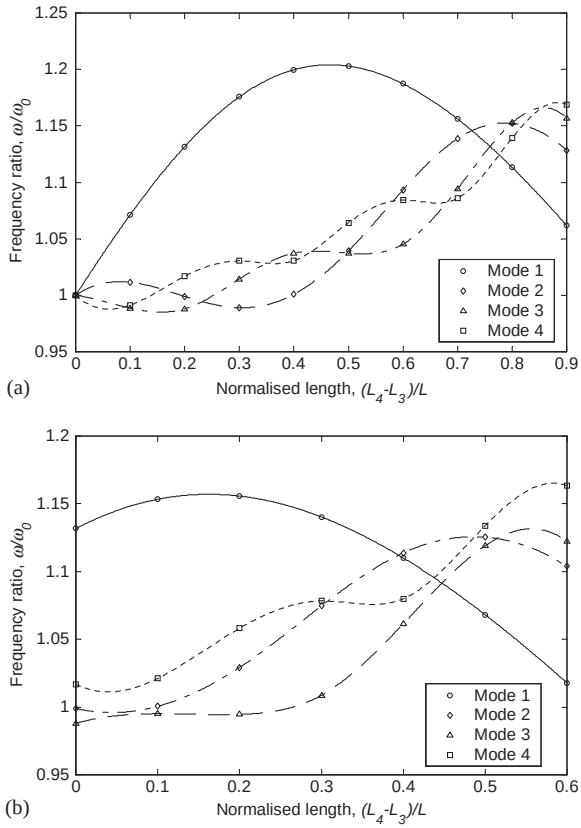

Fig. 5. Frequency ratios for various lengths of $(L_4 - L_3)/L$, with $L_1/L = 0.1$ and (a) $L_2 = L_3 = 0$ and (b) $L_2/L = 0.2$ or $L_3/L = 0.3$. Points indicate calculated values while lines indicate trends.

the region from $0.1L$ to $0.6L$. Since the first mode shape for a cantilever beam experiences the largest flexure near the hub and low flexure elsewhere, these observations support the theory presented above. In this shape, although the stiffening effects dominate when a patch is placed close to the fixed end, the inertia effects become increasingly significant as the patch extends towards the tip. Obviously, this stiffening effect is not present in the study by Chan et al. [6], hence their observation of decreasing frequencies with distributed mass size. For the higher mode shapes, the stiffening effects of the patches seem to dominate and the inertia effects appear to be less significant as demonstrated by the overall increase in the frequencies with patch size. However, the combination of the stiffening and the inertia effects results in localized fluctuations in the frequency ratios as illustrated in these figures.

The dynamic behaviour of composite beams therefore appears to follow the trend that patches placed in regions of low modal flexure contribute little to beam stiffening but significantly to beam mass. This tends to decrease the natural frequency. Patches located in regions of high modal flexure contribute significantly to the composite beam stiffness and so tend to increase the natural frequency. However, patches always contribute in some degree to the effects of both mass and

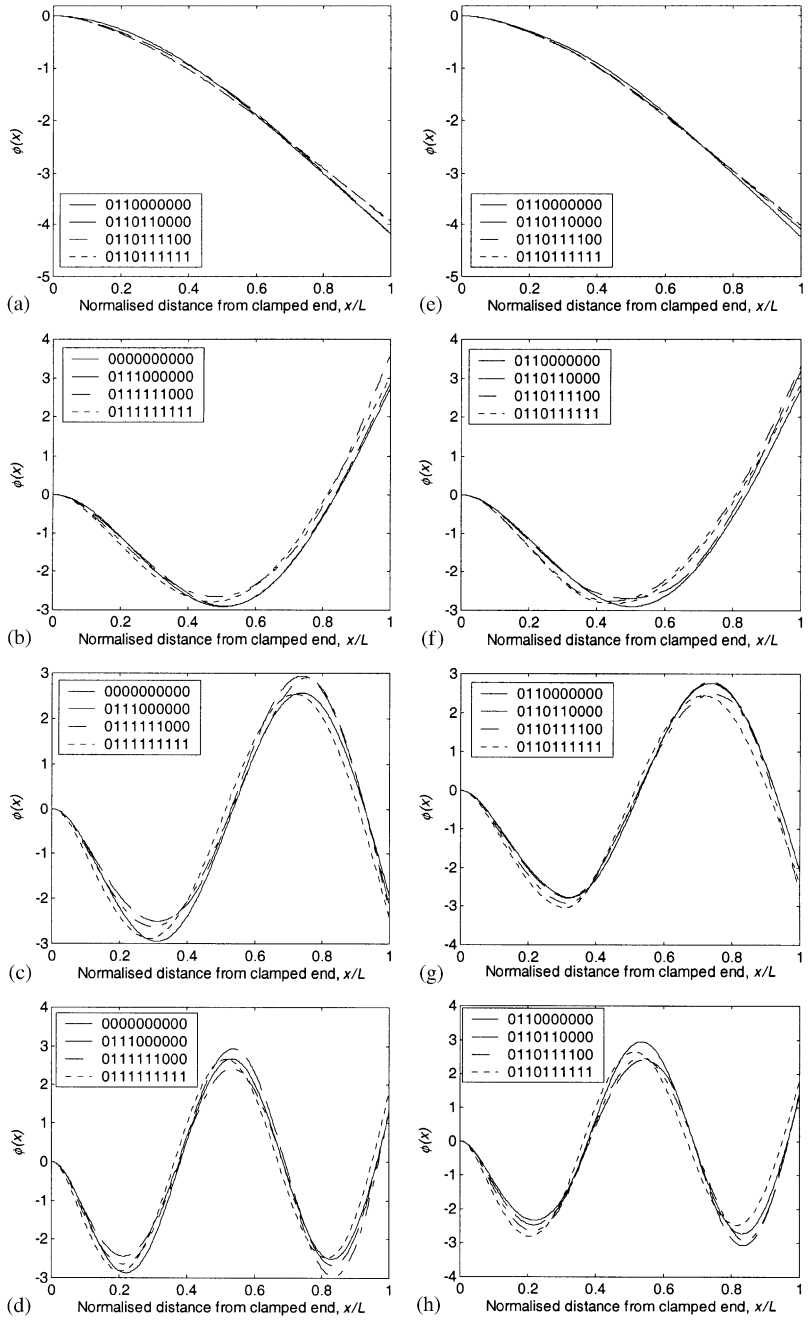

Fig. 6. First four mode shapes for various arrangements using (a)–(d) a single PZT and (e)–(h) 2 PZTs.

stiffness on beam vibration regardless of position. It is this conflict between the effects of mass and stiffness, which warrants exact determination of natural frequencies using computational methods as described in the present investigation.

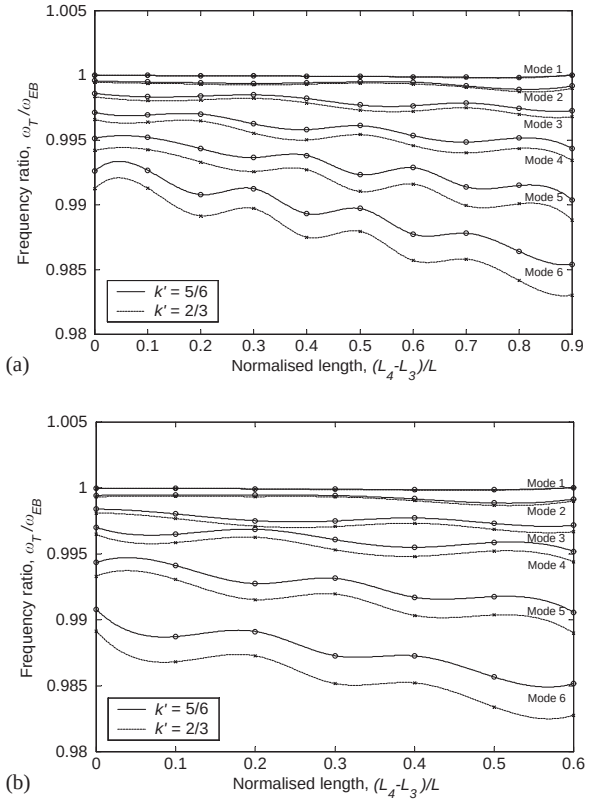

Fig. 7. Timoshenko vs. Euler–Bernoulli frequency ratios for various lengths of $(L_4 - L_3)/L$, with $L_1/L = 0.1$ and (a) $L_2 = L_3 = 0$ or (b) $L_2/L = 0.2$ and $L_3/L = 0.3$. Points indicate calculated values while lines indicate trends.

3.2. Shear effects

From the Timoshenko beam equations, it is also possible to consider the effects of shear in the model for further insight into how the natural frequencies vary with patch position. To this end, the plots in Fig. 7 show the ratios of the natural frequencies obtained using the Timoshenko model against those obtained from an equivalent Euler–Bernoulli model in which shear effects are neglected. The value of the shear parameter k' is also varied between $\frac{5}{6}$ as proposed by such researchers as Cowper [13] and $\frac{2}{3}$ as originally suggested by Timoshenko [14]. This results in two ratio plots for each of the six modes considered in the plot.

As may be seen from Figs. 7(a) and (b), the Timoshenko natural frequencies, ω_T, are in all cases here considered smaller than the respective Euler–Bernoulli natural frequencies, ω_{EB}. For the first mode of vibration, the difference between the two models is marginal, however as the mode number increases the differences become more pronounced. For mode six, the difference approaches 2%, which corresponds to nearly 60 rad/s for the beam under consideration. The difference between the two Timoshenko models for the different shear parameters also becomes more pronounced for higher modes, reaching 0.25% for mode 6. In all cases here shown the

model using a value of $\frac{2}{3}$ for the shear parameter has lower natural frequencies than for that using a value of $\frac{5}{6}$.

Also prominent in the plots in Fig. 7 are similar rippling patterns to those observable in Fig. 5. Since the Euler–Bernoulli model itself here includes the stiffening and inertial effects of the patches, the waves in these plots must therefore be produced by the inclusion of shear.

4. Conclusions

A closed-form approach to the modelling of composite structures such as those formed by bonding piezoceramic patches to the surface of beams has been presented. Segmentation of the structure into numerous smaller beams of uniform beam properties allowed separate mode shapes of vibration to be evaluated for each segment. When placed end-to-end, these yielded the overall mode shapes for the entire beam. This approach may be used for any configuration of patches and is desirable for controller design for structures employing distributed actuation. The effects of placement of PZT patches on the modal characteristics of a cantilever beam have also been described, as have the effects of including shear and of variation in the shear parameter.

Appendix A. Nomenclature

x	axial co-ordinate
t	time
w	transverse deflection
ψ	angle of rotation
β	shear distortion
Q	shear force
M	bending moment
EI	flexural rigidity
ρ	mass per unit volume
A	cross-sectional area
I	moment of inertia
k'	shear coefficient
G	shear modulus
Φ	deflection spatial co-ordinate
Ψ	angular rotation spatial co-ordinate
$q(t)$	generalized time co-ordinate
$A, B, C, D, \alpha, \beta, f_\alpha, f_\beta$	mode shape constants
m	number of segments
n	number of modes
s	segment number
μ	division boundary location
L	link length
h	link height

b	link breadth
t_b	link thickness
o_t	tip mass offset
M_t	tip mass
I_t	tip inertia
F	characteristic matrix
V	coefficient vector
ω	natural frequency
i	mode number
Λ	eigenvalues of F

References

[1] E.F. Crawley, J. deLuis, Use of piezoelectric actuators as elements of intelligent structures, American Institute of Aeronautics and Astronautics Journal 25 (1987) 1373–1385.
[2] E. Garcia, D.J. Inman, J. Dosch, Vibration suppression using smart structures, Smart Materials and Structures 24 (1991) 167–171.
[3] M. Gu, S.F. Asokanthan, Combined discrete-distributed control of a single-link flexible manipulator using a Lyapunov approach, American Society of Mechanical Engineering, Journal of Dynamic Systems, Measurement and Control 121 (1998) 448–456.
[4] S.M. Yang, Y.J. Lee, Modal analysis of stepped beams with piezoelectric materials, Journal of Sound and Vibration 176 (1994) 289–300.
[5] K.T. Chan, X.Q. Wang, Free vibration of a Timoshenko beam partially loaded with distributed mass, Journal of Sound and Vibration 206 (1997) 353–369.
[6] K.T. Chan, X.Q. Wang, T.P. Leung, Free vibration of beams with two sections of distributed mass, Journal of Vibration and Acoustics 120 (1998) 944–948.
[7] A. Joshi, Free vibration characteristics of variable mass rockets having large axial thrust/acceleration, Journal of Sound and Vibration 187 (1995) 727–736.
[8] O.J. Aldraheim, T. Singh, R.C. Wetherhold, Optimal size and location of piezoelectric actuator/sensors: practical considerations, Journal of Guidance and Control 23 (2000) 509–515.
[9] L. Meirovitch, Principles and Techniques of Vibrations, Prentice-Hall, Englewood Cliffs, NJ, 1997.
[10] T.C. Huang, The effect of rotatory inertia and of shear deformation on the frequency and normal mode equations of uniform beams with simple end conditions, Journal of Applied Mechanics 28 (1961) 579–584.
[11] M. Gu, Combined Discrete-Distributed Control of a Two-Link Flexible Manipulator, PhD Thesis, Department of Mechanical Engineering, The University of Queensland, Queensland, 2000.
[12] M.W.D. White, G.R. Heppler, Proceedings of the American Control Conference A Timoshenko Model of a Flexible Slewing Link, 1995.
[13] G.R. Cowper, The shear coefficient in Timoshenko's beam theory, Journal of Applied Mechanics 33 (1966) 335–340.
[14] S. Timoshenko, Strength of Materials: Part 1, D. Van Nostrand Company, Princeton, NJ, 1940.